PNAS RESEARCH ARTICLE | PHYSICS

Detecting the exponential relaxation spectrum in glasses by high-precision nanocalorimetry

Lijian Song[a,b], Yurong Gao[a,b], Peng Zou[a,b], Wei Xu[a,b], Meng Gao[a,b], Yan Zhang[a,b], Juntao Huo[a,b,1], Fushan Li[c], Jichao Qiao[d], Li-Min Wang[e], and Jun-Qiang Wang[a,b,1]

Edited by David Weitz, Harvard University, Cambridge, MA; received February 17, 2023; accepted April 16, 2023

Nonexponential relaxations are universal characteristics for glassy materials. There is a well-known hypothesis that nonexponential relaxation peaks are composed of a series of exponential events, which have not been verified. In this Letter, we discover the exponential relaxation events during the recovery process using a high-precision nanocalorimetry, which are universal for metallic glasses and organic glasses. The relaxation peaks can be well fitted by the exponential Debye function with a single activation energy. The activation energy covers a broad range from α relaxation to β relaxation and even the fast γ/β' relaxation. We obtain the complete spectrum of the exponential relaxation peaks over a wide temperature range from $0.63T_g$ to $1.03T_g$, which provides solid evidence that nonexponential relaxation peaks can be decomposed into exponential relaxation units. Furthermore, the contribution of different relaxation modes in the nonequilibrium enthalpy space is measured. These results open a door for developing the thermodynamics of nonequilibrium physics and for precisely modulating the properties of glasses by controlling the relaxation modes.

glasses | non-exponential relaxation | exponential relaxation spectrum | nanocalorimetry

Significance

Understanding the nature of glasses are one of the most interesting kernels in condensed matter physics. Glassy materials usually exhibit different types of relaxation modes, which are coupled with each other and exhibit nonexponential characteristics. There is a well-known hypothesis that nonexponential relaxations should be composed of a series of exponential relaxation events. However, it is still lack of critical experimental evidence. Here, we provide solid evidence that the nonexponential relaxation peaks in glasses are composed of series of exponential relaxation units. The quantitative measurement and precise modulation of these exponential relaxation units not only provide insights into understanding the nature of glasses but also provide opportunities for enhancing the properties.

Glassy states can be formed in various materials with different types of bonding characteristics, e.g., oxides, alloys, molecules, and polymers (1–4). The nature of glasses and glass transition are one of the most interesting and deepest problems in condensed matter physics. Owing to the nonequilibrium nature, atoms in glasses exhibit extra collective motions besides phonons, e.g., relaxations (1, 5, 6). Studying the relaxation behaviors is of special interests for understanding the nature of glasses (7–9). The relaxations are closely related to atomic diffusion (10, 11), structural heterogeneity (12, 13), mechanical properties (14–16), and the crystallization behavior (17–19). To date, several types of relaxation modes have been identified, e.g., primary α relaxation, slow β relaxation, γ/β' relaxation, and Boson peaks (6, 15, 20). However, the physical description of the relaxation kinetics is far less comprehensive than that of the lattice vibrations in crystals.

One of the vital fundamental challenges is why relaxations usually exhibit nonexponential behavior (8, 21, 22), which could be described by the phenomenological Kohlrausch–Williams–Watts or Havriliak–Negami equations (23–25). The nonexponential behavior is believed to be associated with the heterogeneous structure of glasses. The local regions in glasses may obey various exponential laws, but the superposed state exhibits a nonexponential characteristic (4, 26–29). Pioneering works based on hole-burning technology provide a clue that the broadened relaxation spectra may originate from a distribution of exponential kinetics or Debye responses (30–33). However, a systematic exponential relaxation spectrum has not been reported. Recent dielectric experiments by Richert et al. (34, 35) show that the recovery process exhibits exponential characteristics, which would be helpful for determining the complete exponential relaxation spectrum.

In this work, the enthalpy relaxation peaks after a short-time annealing were measured using high-precision nanocalorimetry Differential scanning calorimetry (Flash DSC) (36–38) for a model metallic glass ($Au_{49}Cu_{26.9}Ag_{5.5}Pd_{2.3}Si_{16.3}$). It covers a very wide temperature range from 253 K to 413 K, i.e., 0.63 T_g to 1.03 T_g, with the glass transition temperature T_g = 401 K. We show that the relaxation heat flow peaks have well-defined spectrum characteristics, which follows the exponential Debye form. The quantitative contributions of various exponential relaxation components are measured in the temperature–enthalpy space.

Results

DSC, especially recently developed flash nanocalorimetry (36–39), provides a high-precision method that can detect very small heat flow responses when the enthalpy state changes (39–42). Herein, we measured the enthalpy relaxation kinetics based on a perturbation methodology to minimize the coupling effect between different relaxation

Author contributions: L.S., J.H. and J.-Q.W. designed research; L.S., Y.G., and P.Z. performed research; L.S., W.X., M.G., Y.Z., J.H., F.L., J.Q., L.-M.W., and J.-Q.W. analyzed data; and L.S., J.H., J.Q., L.-M.W., and J.-Q.W. wrote the paper.

The authors declare no competing interest.

This article is a PNAS Direct Submission.

[1]To whom correspondence may be addressed. Email: huojuntao@nimte.ac.cn or jqwang@nimte.ac.cn.

This article contains supporting information online at https://www.pnas.org/lookup/suppl/doi:10.1073/pnas.2302776120/-/DCSupplemental.

Published May 8, 2023.

modes. The schematic plot is shown in Fig. 1*A*, the sample was measured at cooling rate R_c=10,000 K/s and heating rate R_h = 1,000 K/s. In Fig. 1*B*, the sample preannealed at T_a = 303 K for a short time (i.e., t_a = 5 s) exhibits an extra endothermic peak immediately above T_a compared to the as-cooled glass. The relaxation peak was obtained by subtracting the as-cooled heat flow trace, as shown in the inset of Fig. 1*B*. The routes of aging and recovery are indicated by blue and red arrows, respectively, as shown in Fig. 1*C*. For the same enthalpy, the onset of structural recovery shifts to higher temperature with the annealing temperature increases from T_{a1} to $T_{a3.}$ Similarly, the recovery route also shifts to higher temperatures with the decrease of enthalpy at a given temperature T_{a1}. The subsequent reheating route of annealed sample follows the route of isothermal process (T_a) until recovery is activated. Thus, the recovery process and the aging process should have a one-to-one relationship. Hereafter, we use the recovery heat flow peaks to represent the corresponding aging effect.

Interestingly, if we plot the heat flow peaks of samples annealed for t_a = 5 s at T_a = 273 to 393 K in a semi-logarithmic diagram, as shown in Fig. 2*A*, the contour shows a primary α relaxation peak accompanied with a broad β relaxation shoulder. A similar heat flow peak spectrum can be also constructed for the sample annealed at a given temperature for various times t_a, as shown in Fig. 2*B*. The contour of relaxation peaks of sample annealed at T_a = 253 K for t_a = 20, 50, 100, 200, 500, 1,000, 2,000, 5,000 s, 303 K for t_a = 20, 50, 100, 200, 500, 1,000, 2,000, 5,000, 10,000 s, 318 K for t_a = 2,000, 5,000, 10,000 s and 363 K for t_a = 100, 200, 500, 1,000, 2,000, 5,000 s exhibits a primary α relaxation peak and a broad β relaxation shoulder, which is similar with the DMA spectrum in Fig. 2*C*. It is worthy to note that this phenomenon is also observed in other glassy materials, including metallic glass, polymer glass and small molecule glass (*SI Appendix*, Figs. S2–S6), which suggests its universality in glasses.

Fig. 2 provides the experimental evidence that the nonexponential broad relaxation peaks (e.g., β relaxation and α relaxation) can be decomposed into a series of relaxation peaks, especially beyond the intermediate temperatures. For relaxation peaks at intermediate temperatures, a minor excess wing-like signal is detected in addition to the main peak. But the excess wing has been greatly depressed by about 70% compared to the β relaxation peaks at low temperature (e.g., 358 K), which suggest that β relaxation and α relaxation has been greatly decomposed. To better illustrate the contour of heat flow traces, the temperature-dependent loss modulus (E'') at a driving frequency of f = 2 Hz for the Au-based metallic glass was given in Fig. 2*C*. The loss modulus curve shows a pronounced α relaxation peak with a β relaxation shoulder at lower temperatures, which is consistent with previous results (43–46). A general nonexponential Havriliak–Negami (HN) equation and an exponential Debye equation (47, 48) are used to fit the DMA curve:

$$\text{HN equation: } E = E_u + \frac{E_u - E_r}{[1+(i\omega\tau)^a]^b}, \quad [1]$$

$$\text{Debye equation: } E = E_u + \frac{E_u - E_r}{1+i\omega\tau}, \quad [2]$$

where E is the complex modulus, E_u denotes the unrelaxed modulus, E_r is the relaxed modulus, i represents the imaginary part, ω is the angular frequency, τ is the characteristic relaxation time, a and b are the parameters ranging between 0 and 1, respectively. The fitting from the Debye model with a single relaxation time or activation energy is much narrower than either the α relaxation peak or β relaxation peak. However, the nonexponential HN equation gives a good fitting to the overall experimental curve by involving a distribution of relaxation times. Even though DMA can sensitively detect the inelastic mechanical response in glasses, the applied strain may cause inharmonic effects (49) that make the different relaxation peaks broad and less distinguishable. In other word, the contour of these heat flow curves is similar with the DMA loss modulus curve, reflecting the nonexponential peak is successfully decomposed into subpeaks.

It would be useful to study whether the heating flow peaks exhibit nonexponential or exponential characters. In the recent work (34), it is proposed that the recovery process would show exponential characteristics. To verify this, we tried to use the Debye equation to fit each relaxation peak, as shown in Fig. 3 *A* and *C*. The classical Debye equation with a single relaxation time is given as (30, 50):

$$Q(t) = Q_0\left[1 - exp\left(-\frac{t}{\tau(T)}\right)\right] \quad [3]$$

For a continuous heating process, it gives

$$\begin{aligned} Q(t) &= Q_0\left[1-\exp\left(-\int_{t_s}^{t}\frac{dt}{\tau(T)}\right)\right] \\ &= Q_0\left[1-\exp\left(-\int_{T_s}^{T}\frac{dT}{R_b\tau(T)}\right)\right], \end{aligned} \quad [4]$$

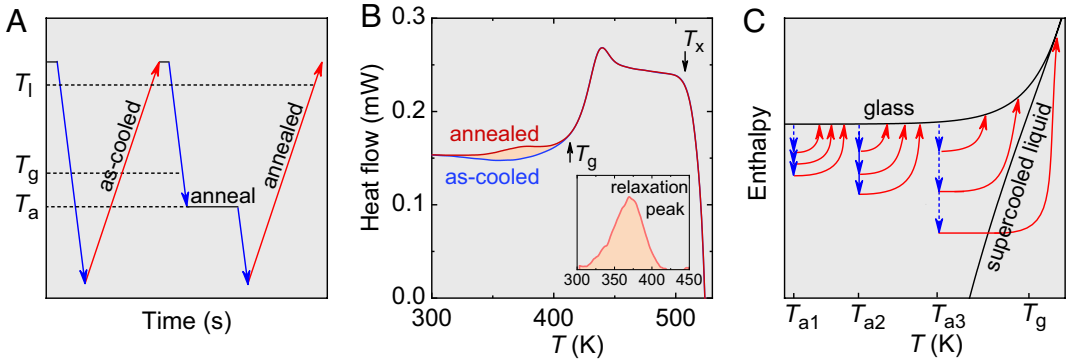

Fig. 1. Thermal protocols of sample. (*A*) The temperature–time protocols with cooling rate of 10,000 K/s and heating rate of 1,000 K/s. The melt is held isothermally at 673 K (29 K higher than T_l= 644 K) for 5 s before quenching to guarantee the melts reach equilibrium state. (*B*) DSC traces of the as-cooled sample and the sample annealed at T_a = 303 K for t_a = 5 s. The inset shows the relaxation peak obtained by subtracting the two DSC traces. The glass transition temperature (T_g) and crystallization temperature (T_x) are marked by arrows. (*C*) Schematic of enthalpy changes at temperatures T_{a1}, T_{a2}, T_{a3}. The blue arrows illustrate structural relaxation during isothermal annealing and the red arrows illustrate structural recovery process during reheating.

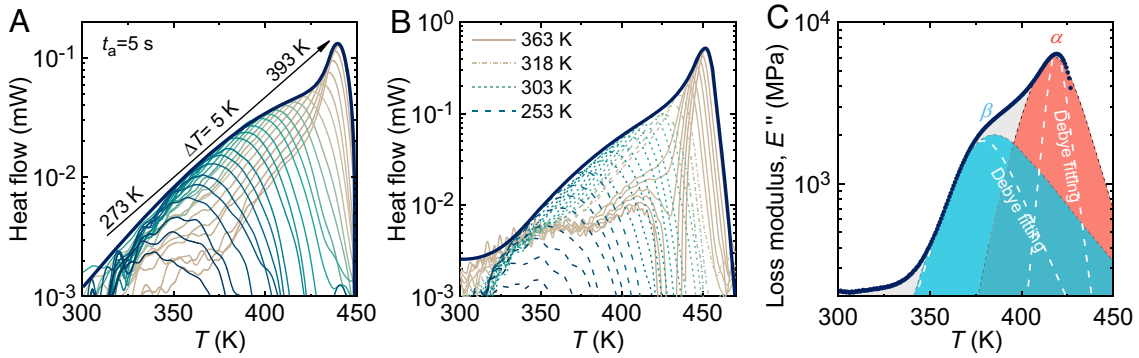

Fig. 2. Spectrum of relaxation peaks. (*A*) Heat flow peaks for the samples being annealed at T_a = 273 to 393 K for t_a = 5 s with a temperature interval of 5 K. (*B*) Heat flow peaks for the samples being annealed at T_a = 253 K for t_a = 20, 50, 100, 200, 500, 1,000, 2,000, 5,000 s; at 303 K for t_a = 20, 50, 100, 200, 500, 1,000, 2,000, 5,000, 10,000 s; at 318 K for t_a = 2,000, 5,000, 10,000 s; and at 363 K for t_a = 100, 200, 500, 1,000, 2,000, 5,000 s, respectively. Along with the increase of annealing time, the relaxation peak shifts to higher temperatures. (*C*) Temperature-dependent loss modulus at f = 2 Hz and R_h = 0.05 K/s. The dashed curve with shaded regions represents the HN fittings for α relaxation (with E^* = 340 kJ/mol) and β relaxation (with E^* = 86 kJ/mol), while the dashed white curves represent the Debye fittings.

where Q_0 is a constant, $\tau(T)$ is the temperature-dependent characteristic relaxation time, t_s is the start time and T_s is the start temperature, R_h is heating rate. The T-dependent relaxation time in both Arrhenius form $\tau = \tau_0 \exp(E^*/RT)$ and in Vogel–Fulcher–Tammann (VFT) form $\tau = \tau_0 \exp[DT_0/(T-T_0)]$ (51) are calculated, where E^* is the activation energy, R is the gas constant, τ_0 represents the time scale in glass, D is the strength parameter and T_0 defines the low temperature limit (see details in *SI Appendix*, Supplementary Materials).

The activation energy derived from Debye fitting E^*_{Debye} is given in Fig. 3*B*. When T_a is above 370 K, E^*_{Debye} is about 350 to 420 kJ/mol, which is close to the classical α relaxation barrier $E^*_\alpha = mRT_g\ln 10$ = 340 to 400 kJ/mol with the fragility of glass-forming liquid is m = 45 to 52 (52–54). When T_a is below 370 K, E^*_{Debye} decreases sharply to below 150 kJ/mol and reaches 44 kJ/mol at 273 K. The classical β relaxation barriwer is $E^*_\beta = (26 \pm 4)RT_g$ = 73 to 100 kJ/mol (41, 55, 56) and the γ/β' relaxation barrier is usually between 20 to 60 kJ/mol (14, 57, 58). This suggests that the β and γ/β'

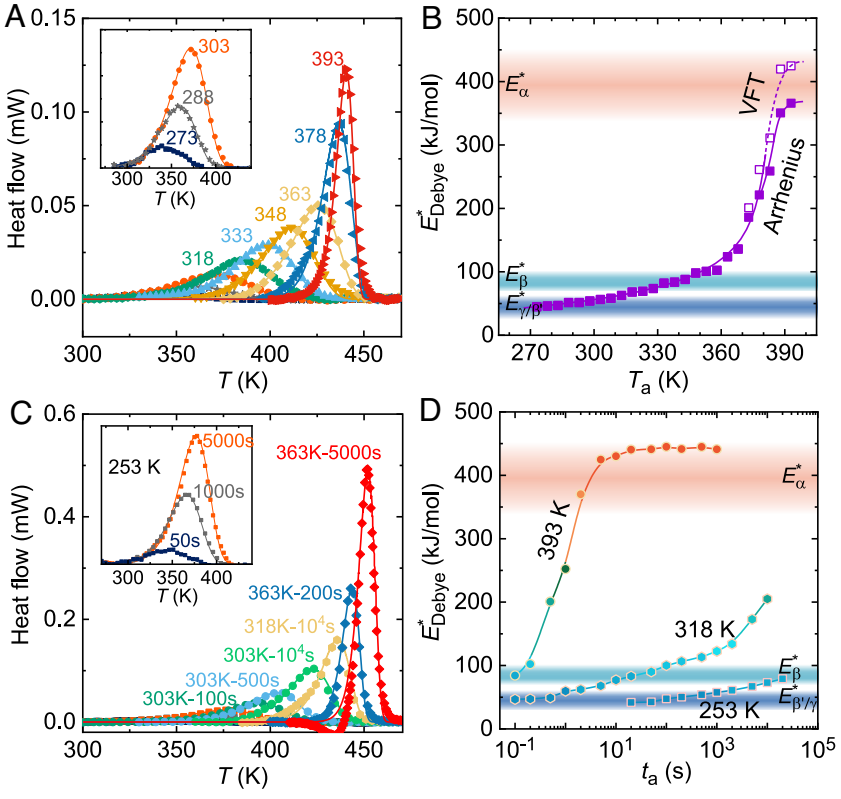

Fig. 3. Relaxation peaks measured by high-precision nanocalorimetry and Debye analysis of the relaxation peaks. (*A*) Representative heat flow data (solid symbols) at T_a = 273 to 393 K for t_a = 5 s fitted using the Debye model (solid curves). (*B*) Annealing-temperature (T_a)-dependent activation energy derived from the Debye fitting, E^*_{Debye}. The open symbols are determined by Vogel–Fulcher–Tammann (VFT) equation and the solid symbols are determined by Arrhenius equation. The shaded areas denote the classical activation energies for γ/β', β, α relaxations, respectively. (*C*) Representative heat flow data (solid symbols) at four representative temperatures fitted using the Debye model (solid curves). The squares: T_a = 253 K for t_a = 50, 1,000, 5,000 s. The circles: T_a = 303 K for t_a = 100, 500, 10,000 s. The hexagons: T_a = 318 K for t_a = 10,000 s. The diamonds: T_a = 363 K for t_a = 200, 5,000 s. (*D*) E^*_{Debye} versus annealing time for samples annealed at three representative temperatures.

relaxation events are detected. We can see that the E_{α}^{*} determined from VFT equation is slightly larger than that from the Arrhenius equation, while the E_{β}^{*} are almost the same from the two equations.

On the other hand, for a given temperature, the relaxation peaks shift to high temperature with the increases of annealing time, as shown in Fig. 3*C*. Representative annealing conditions are given, e.g., t_a = 50, 1,000, 5,000 s at T_a = 253 K; t_a = 100, 500, 10,000 s at T_a = 303 K, t_a = 10,000 s at T_a = 318 K and t_a = 200, 5,000 s at T_a = 363 K. We find that the relaxation peak at a given temperature shows the exponential behavior, which can be fitted well by the Eq. **4**. As shown in Fig. 3*D*, at T_a = 253 K, E_{Debye}^{*} is almost equal to 40 kJ/mol in the initial annealing stage and then progressively increases to 80 kJ/mol. At T_a = 318 K, E_{Debye}^{*} is also equal to 40 kJ/mol in the initial annealing stage, then progressively increases to 80 kJ/mol and increases sharply after 1,000 s. At T_a = 393 K, E_{Debye}^{*} is equal to the β relaxation in the initial annealing stage, then progressively increases to α relaxation and keep constant. The activation energy keeps increasing in the stages of γ/β' relaxation and β relaxation but becomes saturated at α relaxation when the annealing time is long enough. The γ/β' relaxation and β relaxation are related to the local atomic motions that strongly depend on the concentration of free volume. When the annealing time increases, the free volume becomes less and less. This makes the atomic motions becomes slower and the activation energy increases continuously. When the free volume becomes small enough, the atoms have to relax in the way of more collective behavior, i.e., α relaxation. Thus, the activation energy becomes saturated. It is noteworthy that the saturation time of activation energy is much shorter than the equilibrium relaxation time. Given the equilibrium time is 100 s at T_g = 401 K and the fragility is 45, the equilibrium time at 393 K is about 790 s, which is much longer than the saturation time 5 s. These results suggest that the atomic motions have become highly collective far before reaching the equilibrium state.

For applications view, how to precisely modulate the exponential relaxation events is crucial in improving the physical properties. In Fig. 4, we tried to control the exponential relaxation events by step-to-step annealing processes. When the glass is annealed at one temperature (T_a = 403 K for t_a = 0.5 s), only one relaxation peak appears (Fig. 4*A*). When the glass is annealed at two temperatures successively, i.e., first annealed at T_a = 403 K for t_a = 0.5 s then jump to T_a = 363 K for t_a = 0.1 s, another relaxation peak appears on the lower temperature side of the first relaxation peak (Fig. 4*B*). Similarly, when the glass is annealed at three temperatures successively, i.e., first annealed at T_a = 403 K for t_a = 0.5 s then jump to T_a = 363 K for t_a = 0.1 s and finally being annealed at 253 K for t_a = 500 s, a third relaxation peak appears on the lower temperature side of the previous relaxation peaks (Fig. 4*C*). It is note-worthy that the relaxation events stimulated at low temperature annealing don't affect the relaxation events stimulated at high temperatures. These results suggest that the exponential relaxation events can be modulated individually and/or in combination strategies. This provides a chance for precisely changing the glassy state and studying the relaxation-properties relationships.

To measure the contribution of different exponential relaxation events to enthalpy evolution during aging toward equilibrium state, samples were annealed at a wide range of temperatures from 253 K to 413 K for various annealing times. The three-dimensional plot of E_{Debye}^{*} versus enthalpy change and annealing temperature is shown in Fig. 5*A*. For the long-time annealing at high temperatures, the activation energy reaches approximately 350 to 460 kJ/mol, which is close to the activation energy of α relaxation. For medium aging, the activation energy exhibits a plateau at approximately 80 to 120 kJ/mol, which is consistent with the β relaxation activation energy. Notably, for short-time annealing at low temperatures, E_{Debye}^{*} ≈40 kJ/mol, which is close to the activation energy of γ/β' relaxation (15, 57, 58). To better illustrate the evolution of relaxations, a plot of the enthalpy aging in different relaxation modes was constructed, as shown in Fig. 5*B*. The enthalpy data is obtained by subtracting the enthalpy curve of the crystallized sample from the integrated DSC traces. Herein, the glass experiences three stages, i.e., γ/β' relaxation, β relaxation and α relaxation, during isothermal annealing. The amounts of different relaxation modes in enthalpy space are marked by different colors in Fig. 5*B*. The link between E^{*} and $\Delta h = h - h_{crystal}$ describes the survival space of different relaxation modes.

Discussion

Hole-burning experiments provided an experimental evidence that the broad nonexponential relaxation peaks may be composed of exponential components (30–33). However, no experiments succeeded so far in measuring the complete exponential relaxation spectrum. This work provides the experimental cornerstone for the hypothesis. This work also discovers that all the relaxation modes at high temperatures, e.g., α relaxation, β relaxation and γ/β' relaxation, can be decomposed into exponential components.

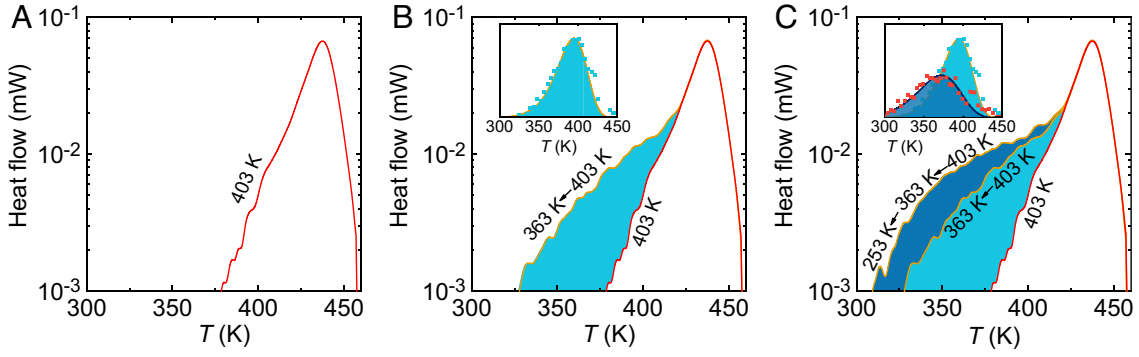

Fig. 4. Controlling the exponential relaxation events in multiple annealing steps. (*A*) Heat flow peak for the glass being annealed at T_a = 403 K for t_a = 0.5 s. (*B*) Heat flow peaks for the glass being annealed successively at T_a = 403 K for t_a = 0.5 s then at T_a = 363 K for t_a = 0.1 s. (*C*) Heat flow peaks for the glass being annealed successively at T_a = 403 K for t_a = 0.5 s then T_a = 363 K for t_a = 0.1 s and finally being annealed at T_a = 253 K for t_a = 500 s. *Insets* show the relaxation peaks triggered from the additional annealing steps.

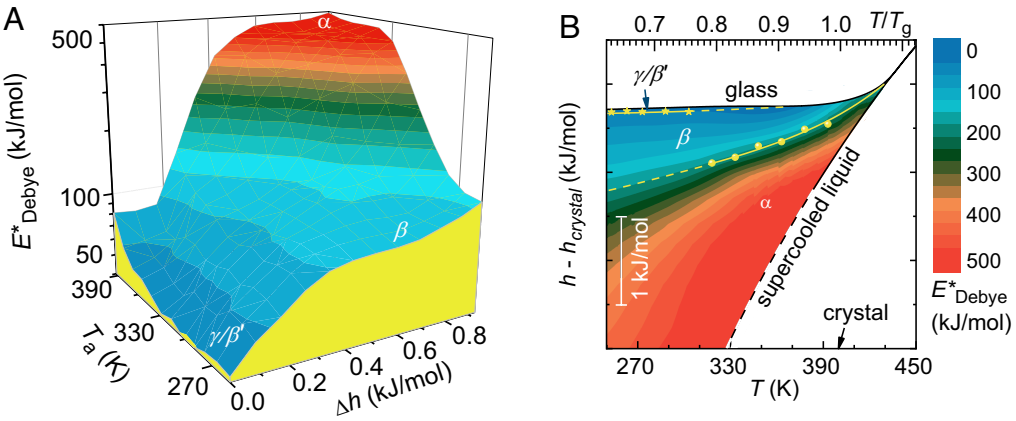

Fig. 5. Contribution of different types of relaxations in enthalpy aging. (*A*) Dependence of activation energy E^*_{Debye} on the enthalpy change of samples annealed at a wide temperature range from 253 K to 413 K. (*B*) Temperature–enthalpy diagram of different relaxation modes. The color contours represent the change in activation energy same as in (*A*). Dashed curves denote the extrapolation based on experimental data. The enthalpies of glass and supercooled liquid have been subtracted by the enthalpy of crystallized sample.

The elastic model for relaxations and glass transition suggests that the nonequilibrium processes are related to the elastic properties (59–61), which originate from the linear atomic interactions. This denotes that the Debye exponential relaxation events probably follow the Boltzmann statistical distribution. We expect that the statistical study of these relaxation units (abbr. relaxun) are helpful for establishing precise description for glassy nonequilibrium thermodynamics.

About the micromechanism of our findings, in the traditional view, glasses are heterogeneous in microstructures that is composed of domains with different characteristic relaxation times according to Richert (34, 62). Our results suggest that the local domains will reach equilibrium accordingly depending on the annealing temperatures and time. The subsequent heating process stimulates the equilibrated micro-domains to high energy states, which is a linear response with exponential kinetics and is accompanied with a Debye relaxation peak. It is noteworthy that the fast rate and high precision of Flash DSC play a critical role in detecting the Debye relaxation peaks. Otherwise, the coupling effect of recovering and aging in slow heating process would yield a much wider relaxation peak.

Conclusions

In summary, we detect exponential relaxation peaks over a wide temperature range from 0.63 T_g to 1.03 T_g, by using a high-precision flash nanocalorimetry. It includes the exponential relaxation components ranging from γ/β' relaxation, β relaxation to α relaxation. We demonstrate that the classical nonexponential relaxation modes can be decomposed into a spectrum of exponential relaxation units, which is a universal characteristic for different types of glasses, e.g., metallic glasses, molecular glasses, polymer glasses and probably oxide glasses. Furthermore, the contributions of various relaxation events in the enthalpy aging process are measured in the temperature–enthalpy space. These results open a door for developing the far-from-equilibrium thermodynamics of glassy materials and for precisely controlling the different relaxation modes and further modulating the properties of glassy systems.

Materials and Methods

The $Au_{49}Cu_{26.9}Ag_{5.5}Pd_{2.3}Si_{16.3}$ (at.%) metallic glass ribbon was prepared by using single roller spinning method under the protection of high-purity Ar atmosphere. The dynamic mechanical properties were measured using a dynamic mechanical analyzer (DMA, TA Q800) at a heating rate of R_h = 0.05 K/s and under sinusoidal tensile stress. The relaxation spectrum of the sample was measured by a high-precision high-rate differential scanning calorimeter (Flash DSC 1, Mettler Toledo). The Flash DSC sample was cut from a melt-spun ribbon with a size of about 50 × 50 × 20 μm and a mass of about 680 ng. During measurement, a flow of high-purity Ar gas (40 mL/min) was applied to protect the sample from oxidation. The sample was prepared by fast cooling (at a rate of 10,000 K/s) from the melt (held at 673 K for 5 s) and annealed isothermally at the target temperatures (T_a = 253 to 413 K) for different time (t_a = 0.1 to 20,000 s).

Data, Materials, and Software Availability. All study data are included in the article and/or *SI Appendix*.

ACKNOWLEDGMENTS. The insightful suggestions from Professor Ranko Richert are appreciated. We acknowledge financial support from the National Key R&D Program of China (2018YFA0703600), National Natural Science Foundation of China (92163108, 52271158, 52222105, 52231006, 52001319, and 51922102), Zhejiang Provincial Natural Science Foundation of China (LGF22E010002, LZ22A030001, and LR22E010004), "Pioneer and Leading Goose" R&D Program of Zhejiang (2022C01023), Ningbo Key Scientific and Technological Project (2019B10051).

Author affiliations: [a]Key Laboratory of Magnetic Materials and Devices, and Zhejiang Province Key Laboratory of Magnetic Materials and Application Technology, Ningbo Institute of Materials Technology and Engineering, Chinese Academy of Sciences, Ningbo 315201, China; [b]Center of Materials Science and Optoelectronics Engineering, University of Chinese Academy of Sciences, Beijing 100049, China; [c]School of Materials Science and Engineering, Zhengzhou University, Zhengzhou 450001, China; [d]School of Mechanics, Civil Engineering and Architecture, Northwestern Polytechnical University, Xian 710072, China; and [e]State Key Laboratory of Metastable Materials Science and Technology, and College of Materials Science and Engineering, Yanshan University, Qinhuangdao, Hebei 066004, China

1. P. G. Debenedetti, F. H. Stillinger, Supercooled liquids and the glass transition. *Nature* **410**, 259–267 (2001).
2. A. L. Greer, New horizons for glass formation and stability. *Nat. Mater.* **14**, 542–546 (2015).
3. W. L. Johnson, J. H. Na, M. D. Demetriou, Quantifying the origin of metallic glass formation. *Nat. Commun.* **7**, 10313 (2016).
4. M. D. Ediger, C. A. Angell, S. R. Nagel, Supercooled liquids and glasses. *J. Phys. Chem.* **100**, 13200–13212 (1996).
5. P. G. Wolynes, V. Lubchenko, *Structural Glasses and Supercooled Liquids: Theory, Experiment, and Applications* (Wiley, 2012).
6. P. Lunkenheimer, U. Schneider, R. Brand, A. Loid, Glassy dynamics. *Contemp. Phys.* **41**, 15–36 (2000).
7. J. C. Dyre, Colloquium: The glass transition and elastic models of glass-forming liquids. *Rev. Mod. Phys.* **78**, 953–972 (2006).
8. J. C. Qiao, J. M. Pelletier, Dynamic mechanical relaxation in bulk metallic glasses: A review. *J. Mater. Sci. Technol.* **30**, 523–545 (2014).

9. W. H. Wang, Dynamic relaxations and relaxation-property relationships in metallic glasses. *Prog. Mater. Sci.* **106**, 100561 (2019).
10. A. Bartsch, K. Ratzke, A. Meyer, F. Faupel, Dynamic arrest in multicomponent glass-forming alloys. *Phys. Rev. Lett.* **104**, 195901 (2010).
11. H. B. Yu, K. Samwer, Y. Wu, W. H. Wang, Correlation between beta relaxation and self-diffusion of the smallest constituting atoms in metallic glasses. *Phys. Rev. Lett.* **109**, 095508 (2012).
12. F. Zhu *et al.*, Intrinsic correlation between β-relaxation and spatial heterogeneity in a metallic glass. *Nat. Commun.* **7**, 11516 (2016).
13. H. Wagner *et al.*, Local elastic properties of a metallic glass. *Nat. Mater.* **10**, 439–442 (2011).
14. H. B. Yu *et al.*, Tensile plasticity in metallic glasses with pronounced beta relaxations. *Phys. Rev. Lett.* **108**, 015504 (2012).
15. Q. Wang *et al.*, Universal secondary relaxation and unusual brittle-to-ductile transition in metallic glasses. *Mater. Today* **20**, 293–300 (2017).
16. S. V. Ketov *et al.*, Rejuvenation of metallic glasses by non-affine thermal strain. *Nature* **524**, 200–203 (2015).
17. T. Ichitsubo *et al.*, Microstructure of fragile metallic glasses inferred from ultrasound-accelerated crystallization in Pd-based metallic glasses. *Phys. Rev. Lett.* **95**, 245501 (2005).
18. L. J. Song *et al.*, Inheritance from glass to liquid: β relaxation depresses the nucleation of crystals. *Acta Mater.* **185**, 38–44 (2020).
19. Y. C. Hu, H. Tanaka, Revealing the role of liquid preordering in crystallisation of supercooled liquids. *Nat. Commun.* **13**, 4519 (2022).
20. Y.-C. Hu, H. Tanaka, Origin of the boson peak in amorphous solids. *Nat. Phys.* **18**, 669–677 (2022).
21. J. M. Pelletier, Dynamic mechanical properties in a $Zr_{46.8}Ti_{13.8}Cu_{12.5}Ni_{10}Be_{27.5}$ bulk metallic glass. *J. Alloys Compd.* **393**, 223–230 (2005).
22. Y. C. Hu *et al.*, Thermodynamic scaling of glassy dynamics and dynamic heterogeneities in metallic glass-forming liquid. *J. Chem. Phys.* **145**, 104503 (2016).
23. R. G. Palmer, D. L. Stein, E. Abrahams, P. W. Anderson, Models of hierarchically constrained dynamics for glassy relaxation. *Phys. Rev. Lett.* **53**, 958–961 (1984).
24. B. Ruta *et al.*, Atomic-scale relaxation dynamics and aging in a metallic glass probed by x-ray photon correlation spectroscopy. *Phys. Rev. Lett.* **109**, 165701 (2012).
25. T. Bennin, J. Ricci, M. D. Ediger, Enhanced segmental dynamics of poly(lactic acid) glasses during constant strain rate deformation. *Macromolecules* **52**, 6428–6437 (2019).
26. R. Richert, Origin of dispersion in dipolar relaxations of glasses. *Chem. Phys. Lett.* **216**, 223–227 (1993).
27. M. D. Ediger, Spatially heterogeneous dynamics in supercooled liquids. *Annu. Rev. Phys. Chem.* **51**, 99–128 (2000).
28. C. Gainaru, R. Böhmer, R. Kahlau, E. Rössler, Energy landscape in molecular glasses probed by high-resolution dielectric experiments. *Phys. Rev. B* **82**, 104205 (2010).
29. R. Richert, Dynamics of nanoconfined supercooled liquids. *Annu. Rev. Phys. Chem.* **62**, 65–84 (2011).
30. F. Alvarez, A. Alegra, J. Colmenero, Relationship between the time-domain kohlrausch-williams-watts and frequency-domain havriliak-negami relaxation functions. *Phys. Rev. B.* **44**, 7306–7312 (1991).
31. X. F. Shi, G. B. McKenna, Mechanical hole burning spectroscopy: Evidence for heterogeneous dynamics in polymer systems. *Phys. Rev. Lett.* **94**, 157801 (2005).
32. B. Schiener, R. Böhmer, A. Loidl, R. V. Chamberlin, Nonresonant spectral hole burning in the slow dielectric response of supercooled liquids. *Science* **274**, 752–754 (1996).
33. K. R. Jeffrey, R. Richert, K. Duvvuri, Dielectric hole burning: Signature of dielectric and thermal relaxation time heterogeneity. *J. Chem. Phys.* **149**, 6150–6156 (2003).
34. R. Richert, J. P. Gabriel, E. Thoms, Structural relaxation and recovery: A dielectric approach. *J. Phys. Chem. Lett.* **12**, 8465–8469 (2021).
35. S. Samanta, R. Richert, Limitations of heterogeneous models of liquid dynamics: Very slow rate exchange in the excess wing. *J. Chem. Phys.* **140**, 054503 (2014).
36. J. E. K. Schawe, J. F. Löffler, Existence of multiple critical cooling rates which generate different types of monolithic metallic glass. *Nat. Commun.* **10**, 1337 (2019).
37. C. Schick, A. Toda, R. Androsch, The narrow thickness distribution of lamellae of poly(butylene succinate) formed at low melt supercooling. *Macromolecules* **54**, 3366–3376 (2021).
38. L. J. Song *et al.*, Activation entropy as a key factor controlling the memory effect in glasses. *Phys. Rev. Lett.* **125**, 135501 (2020).
39. M. Gao, J. H. Perepezko, Separating β relaxation from α relaxation in fragile metallic glasses based on ultrafast flash differential scanning calorimetry. *Phys. Rev. Mater.* **4**, 025602 (2020).
40. S. Vyazovkin, I. Dranca, Probing beta relaxation in harmaceutically relevant glasses by using DSC. *Pharm. Res.* **23**, 422–428 (2006).
41. L. N. Hu, Y. Z. Yue, Secondary relaxation in metallic glass formers: Its correlation with the genuine johari-goldstein relaxation. *J. Phys. Chem. C* **113**, 15001–15006 (2009).
42. J. C. Lee, Calorimetric study of β-relaxation in an amorphous alloy: An experimental technique for measuring the activation energy for shear transformation. *Intermetallics* **44**, 116–120 (2014).
43. R. Bergman, General susceptibility functions for relaxations in disordered systems. *J. Appl. Phys.* **88**, 1356–1365 (2000).
44. Z. Wang, B. A. Sun, H. Y. Bai, W. H. Wang, Evolution of hidden localized flow during glass-to-liquid transition in metallic glass. *Nat. Commun.* **5**, 5823 (2014).
45. J. M. Pelletier, S. Cardinal, J. C. Qiao, M. Eisenbart, U. E. Klotz, Main and secondary relaxations in an au-based bulk metallic glass investigated by mechanical spectroscopy. *J. Alloys Compd.* **684**, 530–536 (2016).
46. Z. Evenson *et al.*, β relaxation and low-temperature aging in a Au-based bulk metallic glass: From elastic properties to atomic-scale structure. *Phys. Rev. B* **89**, 174204 (2014).
47. P. Q. Mantus, Dielectric response of materials extension to the debye model. *J. Eur. Ceram. Soc.* **19**, 2079–2086 (1999).
48. G. G. Raju, *Dielectric loss and relaxation–I* (CRC Press, 2017), pp. 103–156.
49. H. B. Yu, R. Richert, R. Maass, K. Samwer, Strain induced fragility transition in metallic glass. *Nat. Commun.* **6**, 7179 (2015).
50. R. M. Hill, L. A. Dissado, Debye and non-debye relaxation. *J. Phys. C Solid State Phys.* **18**, 3829–3836 (1985).
51. Z. Wang, P. Wen, L. S. Huo, H. Y. Bai, W. H. Wang, Signature of viscous flow units in apparent elastic regime of metallic glasses. *Appl. Phys. Lett.* **101**, 121906 (2012).
52. I. Gallino *et al.*, Hierarchical aging pathways and reversible fragile-to-strong transition upon annealing of a metallic glass former. *Acta Mater.* **144**, 400–410 (2018).
53. J. Q. Wang, Y. Shen, J. H. Perepezko, M. D. Ediger, Increasing the kinetic stability of bulk metallic glasses. *Acta Mater.* **104**, 25–32 (2016).
54. J. Schroers, On the formability of bulk metallic glass in its supercooled liquid state. *Acta Mater.* **56**, 471–478 (2008).
55. J. Schroers, B. Lohwongwatana, W. L. Johnson, A. Peker, Gold based bulk metallic glass. *Appl. Phys. Lett.* **87**, 061912 (2005).
56. K. L. Ngai, S. Capaccioli, Relation between the activation energy of the johari-goldstein beta relaxation and T_g of glass formers. *Phys. Rev. E.* **69**, 031501 (2004).
57. S. Ouyang *et al.*, Chemical independent relaxation in metallic glasses from the nanoindentation experiments. *J. Appl. Phys.* **121**, 245104 (2017).
58. S. Küchemann, R. Maaß, Gamma relaxation in bulk metallic glasses. *Scripta Mater.* **137**, 5–8 (2017).
59. J. Q. Wang, W. H. Wang, Y. H. Liu, H. Y. Bai, Characterization of activation energy for flow in metallic glasses. *Phys. Rev. B* **83**, 012201 (2011).
60. W. H. Wang, The elastic properties, elastic models and elastic perspectives of metallic glasses. *Prog. Mater. Sci.* **57**, 487–656 (2012).
61. J. C. Dyre, W. H. Wang, The instantaneous shear modulus in the shoving model. *J. Chem. Phys.* **136**, 224108 (2012).
62. R. Richert, Heterogeneous dynamics in liquids: Fluctuations in space and time. *J. Phys. Condens. Matter* **14**, R703–R738 (2002).